ORIGINAL ARTICLE

Thermal influence analysis of coatings and contact resistance in turning cutting tool using COMSOL

Carlos A. Corrêa Ribeiro[1] · João R. Ferreira[1] · Sandro M. M. Lima e Silva[1]

Abstract
In machining processes, cutting tools reach temperatures higher than 900 °C, thus deteriorating their mechanical properties. To reduce this problem, cutting tools are coated with materials possessing thermal insulation characteristics. Such coatings benefit machining, providing faster cutting speeds and tool life. However, the heating of the tools is still present. Therefore, in this work, an analysis of the thermal effects of coating in a carbide tool using COMSOL® software is presented. The effects of convection, radiation, and contact resistance between the tool and the tool holder are also considered. The thermophysical properties of the tool elements depend on temperature. Experimental measurements of parameters related to contact resistance were carried out to make the thermal model closer to real situations. The COMSOL program was used to solve the heat diffusion equation using the finite element method. Comparisons of calculated temperatures are presented for the uncoated (substrate only) and coated inserts with aluminum oxide (Al_2O_3) and titanium nitride (TiN), respectively. Coatings fulfill the role of protecting the heat directed to the tool substrate, but at different intensities. While the Al_2O_3 acts as a thermal barrier, retaining heat on the output surface, TiN has a less intense temperature gradient in the space of 10 μm, including a lower temperature on the output surface. The contact resistance raised the temperature on the output surface by 45.2 °C, 39.6 °C, and 39.5 °C for uncoated tools and coated by Al_2O_3 and TiN, respectively.

1 Introduction

The heating phenomenon of cutting tools has attracted engineers' attention since 1925, with publications such as Shore [1]. The study of the thermal field in cutting tools is considered the main factor in the tool lifespan [2] since it reflects the cutting parameters adopted, according to publications such as Grzesik and Nieslony [3]. The cutting speed has the most significant weight among the machining parameters when

✉ Carlos A. Corrêa Ribeiro
cadrianocr@yahoo.com.br

João R. Ferreira
jorofe@unifei.edu.br

Sandro M. M. Lima e Silva
metrevel@unifei.edu.br

[1] Instituto de Engenharia Mecânica - IEM, Universidade Federal de Itajubá - UNIFEI, Campus Prof. José Rodrigues Seabra, Av. BPS, 1303, Itajubá, Minas Gerais 37500-903, Brazil

heating the tool in low and medium values. In addition, its greatest effects occur in the secondary and tertiary cutting areas due to friction with the tool. The high speeds cause the chip to flow through the tool without dissipating heat to the tool, according to Iraola et al. [4]. Papers like Chen et al. [2] show that heat is the main factor affecting the tool integrity since a large amount of heat is concentrated in a small area. For Kaminise et al. [5], many other factors contribute to the tool heating. Some of these factors are the workpiece materials, the tool materials, the presence of coating, the use of coolants, the tool geometry, and even the material of tool holders.

The procedures used to estimate the temperature in cutting tools have also involved analytical methods, according to Machado et al. [6]. Other methods involve experiments, including allied to numerical methods. The experimental methods that can be used to measure the temperature of a cutting tool are the tool-piece thermocouple effect and the use of thermocouples as in the work of Chen et al. [2], Kaminise et al. [5], and Rech et al. [7]. It is also possible to obtain the temperature in a cutting tool through pyrometers or

infrared cameras by measuring thermal radiation emission from the tool [8]. It is possible to estimate the temperature in a cutting tool even with thermosensitive varnishes, which react chemically as a function of the increase in temperature [6]. Each one of these techniques has advantages and disadvantages. In general, experimental methods require specific equipment such as thermocouples, thermal imaging cameras, data acquisition systems, and other instrumentation systems. Thermocouple use, for example, is a simple method, but presents the temperature at a single point, which cannot represent the maximum temperature that occurred in the tool. Infrared cameras allow measuring temperatures without modifying the cutting tool geometry or even without contact with it. However, they only measure on exposed surfaces. Therefore, it is not possible to use it in the presence of cutting fluids or in regions that are not exposed to lens. Varnishes are removed from the tool during the cutting operation and provide a temperature estimation. Since experimental procedures require the use of appropriate equipment, this makes studies more expensive. Moreover, since all experimental methods have some limitations, they are used together with numerical methods, as in Brito et al. [9].

Numerical methods involve the resolution of differential equations, the analytical solutions of which are difficult to obtain. Numerical methods began to be used to study heat cutting tools in the 1970s [10]. In this work, the method used to analyze the temperature in a tool was the finite element method (FEM). The development of hardware and software has led to improvements in numerical methods such as FEM, finite volume method (FVM), boundary element method (BEM), among others, as highlighted by Maliska [11]. Numerical methods are applied not only to study the temperature field in tools but also to estimate the cutting force in machining, as was the case in the work of Coroni and Croitoru [12], in which the authors applied the difference finite method for obtaining the cutting force in an orthogonal model. Another application of numerical methods was to study the contact resistance between solid domains, as was done in Goodarzi et al. [13] and Zheng et al. [14] to improve contact resistance prediction. A variation of the finite element method, known as the spectral method (Fourier space), was applied in Beake et al. [15]. This study evaluated the wear of machining tools in the presence of coolant fluid. According to this work, the coating life can be extended up to 100% due to applying other coating layers on the tool, such as AlCrN-TiAlN. The study also evaluated material fatigue due to tool heating.

In experimental studies, the correct knowledge of the boundary conditions requires separate work. When dealing with cutting tools, it is common to use inverse problem techniques to determine the boundary conditions and the initial domain conditions. Thus, in Brito et al. [9], a study was carried out based on the function specification method,

implemented in MATLAB, combined with the solution of the heat diffusion equation by the FEM. Using the function specification method, it was possible to estimate the heat flux. From this step, the thermal problem of transient three-dimensional heat conduction was solved using the COMSOL program.

The first cutting tools were made of carbon steel. Over the years, other materials appeared, such as synthesized alloys, ceramic materials, and even boron nitride and diamond-based tools, according to Diniz et al. [16]. Even so, cutting tools suffer from heat damage. Therefore, in some situations, cutting fluids are used to smooth the thermal gradient in the tool. However, cutting fluids bring other problems, such as damage to health, in addition to environmental problems [15]. The next step in the machining process evolution was to coat the cutting tool with an external layer of material with low thermal conductivity, using the chemical vapor deposition (CVD) and physical vapor deposition (PVD) processes.

Regarding the use of these coatings, Machado et al. [6] mention that PVD and CVD techniques form coatings with different characteristics, resulting in tools for different machining conditions. Coatings play a dual role in the cutting process. The first is to act as a thermal insulator, and the second is to reduce friction with the part and, consequently, reduce the heat generated. Studies on coatings show that it provides benefits such as reduced flank wear [17]. Some studies mention the limitations of coatings [18], which depending on their composition, cannot withstand temperatures above 600 °C. The coatings also present a different behavior depending on the piece composition, as demonstrated in Aiso et al. [19], where the alloying elements present in the steel (TiCN + Al_2O_3 + TiN) deposited by CVD were studied. This work concluded that different composition pieces, although subtle, can give rise to different tribological and wear behaviors. Bobzin [20] studied the consequences of using coated tools concerning the costs of machining processes. According to this work, the coatings minimize abrasion and diffusion wear. Bobzin [20] noted that 85% of the tools in use today are coated to minimize cutting fluids even while increasing the cutting speed. The structural characteristics of the coatings, including multilayer and nanoparticles, were also discussed. In addition to acting as a thermal barrier [21], the coatings must withstand high dynamic loads and be chemically stable since the tool substrate cannot have all these requirements [22]. According to their study, it was also found in Park et al. [23] that a parameter that defines the coating quality and performance is its adhesion to the substrate. Bar-Hen and Etsion [24] also evaluated the role of the thickness of TiAlN coatings and the effect of substrate roughness on tool wear during turning. According to this work, the coating thickness reduces the tool wear, while a greater roughness in the substrate increases the tool wear. Despite all these desirable characteristics, the coatings also have critical points since they depend on an

interactive process with the substrate, as pointed out by Vereschaka and Grigoriev [25]. In this work, failures in nanostructured multilayer coatings were studied, citing parameters that can lead to failure or the coating premature wear. A parameter related to coating failure is the specific cutting pressure acting on the contact interface between the tool and the workpiece, exceeding the tool plastic limit and coating material. According to Vereschaka and Grigoriev [25], cutting parameters influence the performance of substrate and coating materials.

Systems composed of two or more solid bodies in contact present a sudden variation in temperature at the interface due to contact resistance. This occurs due to the contact surface roughness, which makes it difficult for heat to spread. Roughness means that only a few contact points are between the solids, permeated by interstices of air. Contact resistance is present in any assembly and changes the heat conduction pattern. Since, in the case of tools consisting of an insert and tool holder, its contact is not perfect no matter how small the surface roughness is, making it difficult to dissipate the heat generated during the cutting operation. Procedures have already been proposed to measure contact resistance presented in Mo and Segawa [26] when studying one-dimensional heat conduction between solid surfaces. Factors influencing contact resistance were highlighted in Cui et al. [27]. According to this work, in addition to roughness, other parameters that have to be considered are the contact pressure, the flatness of the surfaces, the microhardness of the materials, and the thermal conductivity of the assembly materials. For Krajinovic et al. [21], these factors must be considered since the contact pressure can lead to plastic deformation of the assembly material, changing the roughness profile at the contact interface, expanding the solid-solid contact, and favoring heat conduction.

The heat flux estimated from Brito et al. [9] was used in this work, by using COMSOL software was possible to calculate the temperature field in the tool, considering the effects of coatings and contact resistance. Comparative analyses of the calculated temperatures were performed for the uncoated and coated insert with aluminum oxide (Al_2O_3) and titanium nitride (TiN). It is noteworthy that for calculating the temperature using the COMSOL software, the temperature-dependent thermophysical properties was considered. One of the main contributions of this work is to consider contact resistance effect in calculating numerical temperature. Therefore, the parameters responsible for its effects, such as surface roughness, microhardness, and contact pressure, were measured to obtain their values in the most realistic way possible. Constriction conductance was calculated using the Cooper-Mikic-Yovanovich (CMY) correlation [28], valid for isotropic rough surfaces. The CMY correlation relates constricting conductance to roughness and pressure load at the contact interface. The interstitial conductance is calculated assuming that the

fluid in the interstices is air; the air thermal conductivity, the average thickness of the gap, and the air parameter were considered. It is also worth highlighting COMSOL software use since it has implemented all the methodology used to calculate the contact resistance. It was observed that when the temperature for the coated insert was calculated considering the contact resistance, there was a significant increase in temperature compared to the uncoated insert.

2 Methodology

In this work, a cutting tool assembly, compound by insert, shim, and tool holder, was modeled. The tungsten carbide (WC) insert dimensions are shown in Fig. 1a. The insert also has a tip radius of 0.8 mm and it is mounted in the tool holder with the help of a shim (Fig. 1b), placed between the insert and its tool holder.

The complete set is shown in Fig. 2. In this assembly, the shim and the tool holder are made of AISI 1045 steel.

To solve the thermal problem, the set is divided into domains so that each domain is part of the set subject to a different boundary condition. As shown in Fig. 3, the S_1 domain is the contact interface between the cutting insert and chip, a region subject to heat flux. S_2 represents the upper surface of the insert, subject to radiation and convection effects. The S_3 domain is the vertical side of the insert subjected to convection and radiation. S_4 is the contact interface between the insert and the fixing clamp, while the domain S_5 indicates the contact interface between the insert and the tool holder.

The S_2 and S_4 domains denote the tool upper surface parts, subject to convection/radiation and contact resistance, respectively. However, initially, these surfaces assume the WC emissivity and roughness characteristics to simulate heat conduction in the absence of coating. Then, S_2 and S_4 domains assume the emissivity and roughness values of materials typically used as coatings, Al_2O_3 and TiN.

Figure 4 shows the domains of the bottom surface of the insert. In this case, S_6 is the contact interface between the cutting insert and the shim, and S_7 is the lower horizontal surface of the insert, also subject to convection and radiation. The S_6 and S_7 domains assume only the WC emissivity and roughness values since coating beyond the insert upper surface is not considered.

The domain of shim and tool holder are presented in Fig. 5. In the shim, there are the domains S_8 for contact with the insert substrate, S_9 for vertical surfaces, and S_{10} for horizontal contact with the tool holder. In the tool holder, its interfaces with the substrate and the shim are S_{11} and S_{12}, respectively. The outer surfaces of the tool holder are designated S_{13}.

The S_1 domain is modeled from an experimental measurement using an image analyzer carried out in Carvalho et al.

Fig. 1 Dimensions of the modeled cutting insert (**a**) and the shim (**b**), in mm

(a)
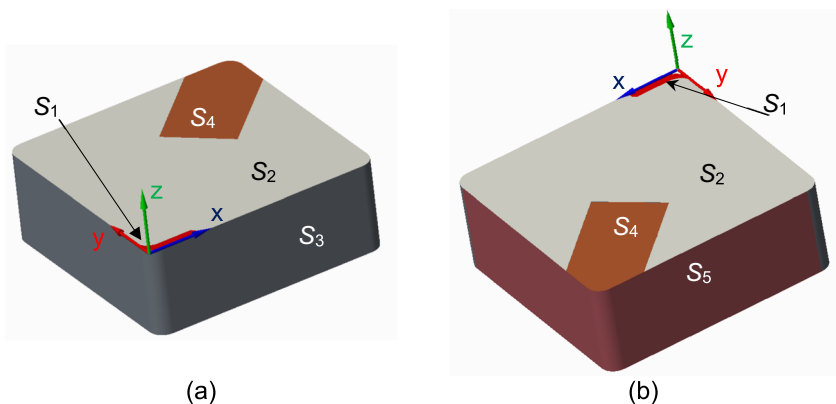
(b)

Insert

Shim

Tool hold
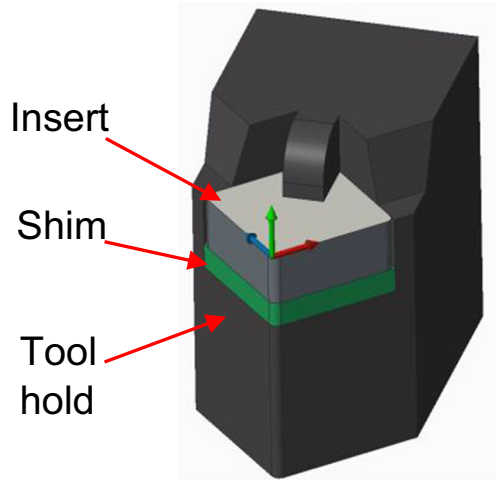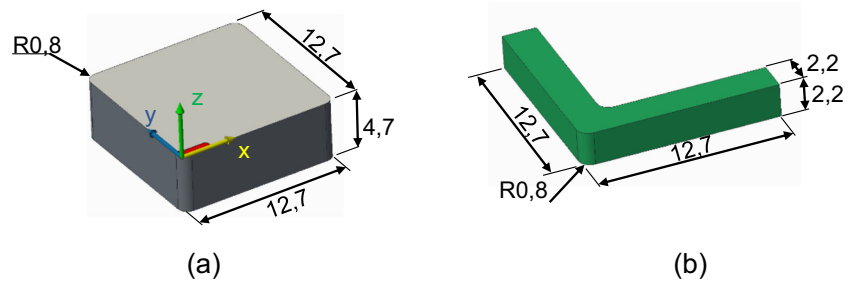
Fig. 2 Cutting tool assembly

[29], and its value is 0.411 mm^2. In Fig. 6, the experimental S_1 region is compared with the one modeled in this work.

2.1 Thermophysical properties

The necessary thermophysical properties are thermal conductivity, specific heat, thermal emissivity of WC, AISI 1045 steel, Al$_2$O$_3$, and TiN. The thermal conductivity of these materials is obtained from Grzesik et al. [30], extracting specific points and performing the curve corresponding fitting. The behavior of thermal conductivity as a function of temperature is shown in Fig. 7.

The specific heat values of WC, AISI 1045 steel, Al$_2$O$_3$, and TiN were calculated from the temperature-dependent thermal diffusivity values obtained from Grzesik et al. [30] and are shown in Fig. 8.

The density values were considered constant and are shown in Table 1 and were also obtained in Grzesik et al. [30].

Based on Jiang et al. [31], the emissivity of WC is treated as dependent on temperature, and its behavior is shown in Fig. 9.

The emissivity of the AISI 1045, Al$_2$O$_3$, and TiN steels was considered constant, and their values were obtained, respectively, from Polozine and Schaeffer [32], Wang et al. [33], and Hou et al. [34] and are shown in Table 2.

2.2 Thermal model

The transient non-linear three-dimensional diffusion equation can describe the thermal model shown in Fig. 2, Eq. (1):

$$\frac{\partial}{\partial x}\left[k(T)\frac{\partial T}{\partial x}\right] + \frac{\partial}{\partial y}\left[k(T)\frac{\partial T}{\partial y}\right] + \frac{\partial}{\partial z}\left[k(T)\frac{\partial T}{\partial z}\right]$$

$$= \rho C_p(T)\frac{\partial T}{\partial t} \tag{1}$$

in what ρ is the density, C_p is the specific heat, and k is the thermal conductivity. The set is divided into domains so that each domain is subject to a specific boundary condition. The domains are shown in Figs. 3 and 4. The boundary conditions of the problem are:
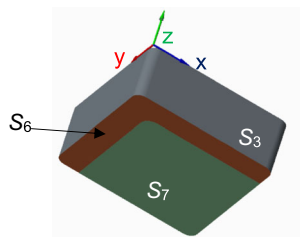
Fig. 3 Insert domains on top and vertical surfaces in front side (**a**) and back side (**b**)

(a)

(b)

Fig. 4 Domains of the bottom surface of the insert

$$-k(T)\frac{\partial T}{\partial z} = q_0'' \text{ em } S_1 \tag{2}$$

and

$$k(T)\frac{\partial T}{\partial \eta} = h(T)(T - T_\infty)$$
$$+ \sigma\varepsilon(T)\left(T^4 - T_\infty^4\right) \text{ em } S_2, S_3, S_7, S_{10} \text{ e } S_{14} \tag{3}$$

The initial condition of the problem is:

$$T = T_\infty \text{ at } t = 0 \tag{4}$$

in which q_0'' is the heat flux, h is the convection coefficient, σ is the Stefan-Boltzmann constant, T is the temperature, T_∞ is the ambient temperature, and t is related to time. In the contacts between the insert and the tool holder, the insert and the shim, and between the shim and the tool holder, there is the presence of contact resistance. COMSOL matches contact resistance using CMY correlation [28]. For this, the Eqs. (5) and (6) are presented:

$$k_1\left(\frac{\partial T_1}{\partial x} + \frac{\partial T_1}{\partial y} + \frac{\partial T_1}{\partial z}\right) = -h_{rc}(T_2 - T_1) \tag{5}$$

and

$$k_2\left(\frac{\partial T_2}{\partial x} + \frac{\partial T_2}{\partial y} + \frac{\partial T_2}{\partial z}\right) = -h_{rc}(T_1 - T_2) \tag{6}$$

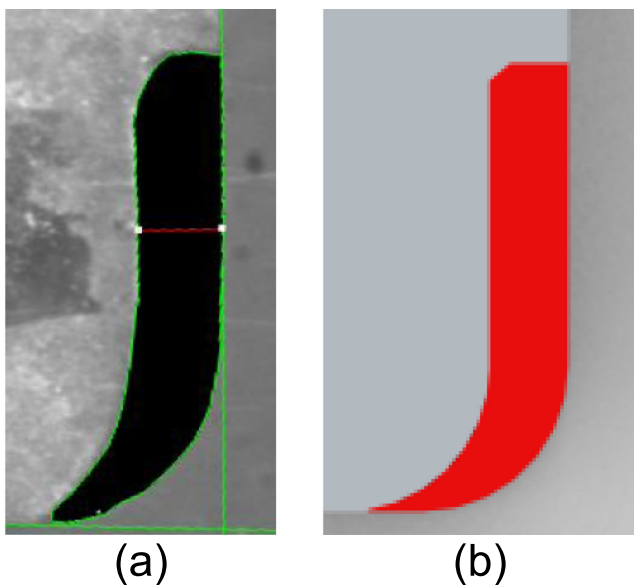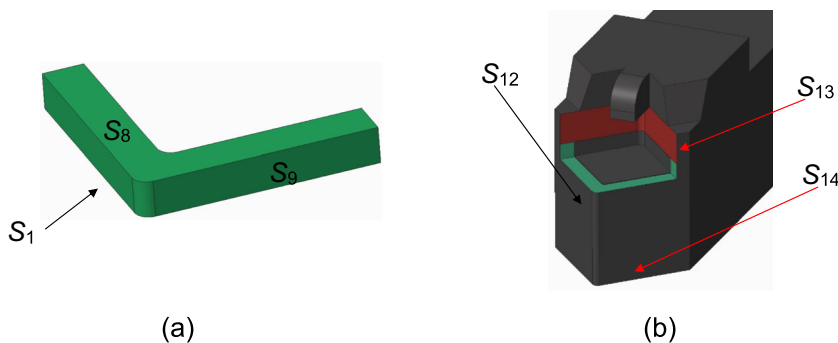**Fig. 5** The domain of shim (**a**) and tool holder (**b**)

(a)

(b)

(a)   (b)

Fig. 6 The comparison between the insert contact area in the experimental model (**a**) and the numerical model (**b**)
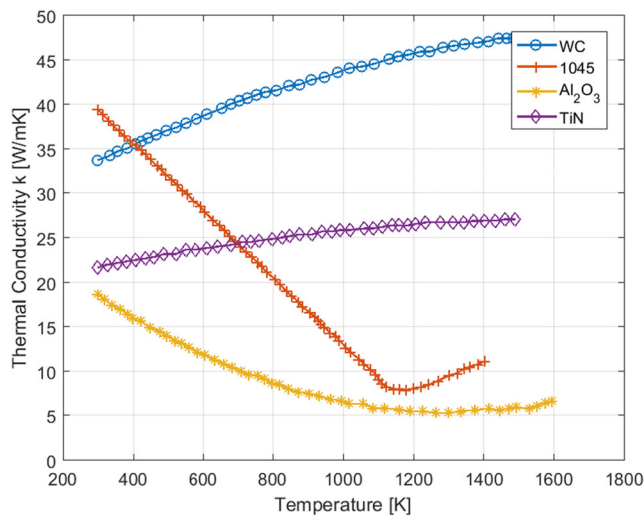

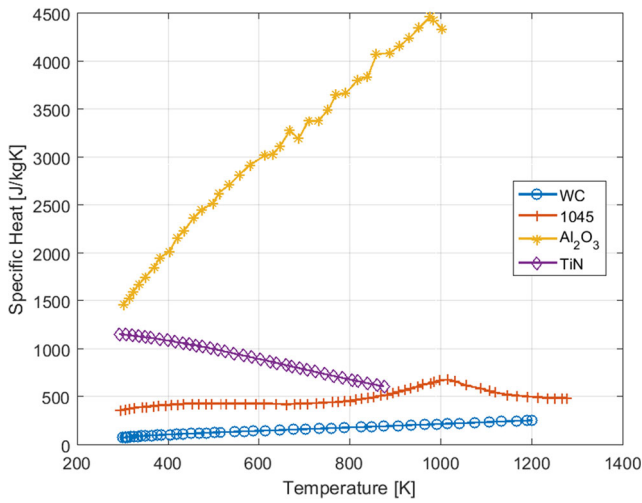**Fig. 7** Thermal conductivity of WC, 1045, Al_2O_3, and TiN steel materials

Fig. 8 Specific heat for the WC, AISI 1045 steel, Al$_2$O$_3$, and TiN

Fig. 9 Thermal emissivity for the WC

whereas

$$h_{rc} = h_g + h_c \tag{7}$$

The term h_{rc} is the combination of two portions in which h_g is the convection coefficient of the fluid present in the interstices of the contact face and h_c is calculated using Eq. (8). The properties of the contact surfaces are defined through the average surface roughness, m_{asp}, the inclination of the roughness slopes, σ_{asp}, and microhardness of the softer surface, H_c. The contact pressure P is also necessary for the calculation:

$$h_c = 1.25 k_c \frac{m_{asp}}{\sigma_{asp}} \left(\frac{P}{H_c} \right)^{0.95} \tag{8}$$

In Eq. (8), the term k_c is the harmonic mean of the two material thermal conductivities in contact, being calculated using Eq. (9):

$$k_c = \frac{2 k_1 k_2}{k_1 + k_2} \tag{9}$$

2.3 Direct problem resolution

In this work, the thermal problem is treated as a direct problem. The boundary and initial conditions are known, using the heat flux values estimated by Brito et al. [9]. The heat
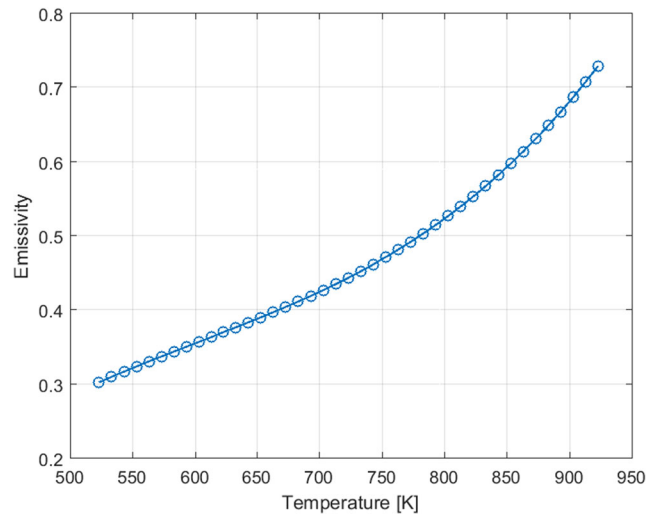
diffusion equation was solved using the COMSOL software, a graphical interface software, based on the finite element method. The set was discretized by tetrahedral elements, not structured. The uncoated model was discretized in 283,448 elements, and the coated model was discretized in 310,952 elements.

In COMSOL, an attempt was made to simulate the heating of the set within an interval of 84 s and with a time increase of 0.5 s. The numerical method used for solving the heat diffusion is the backward differentiation formula (BDF), an implicit method. In this method, the solution involves the variable of interest in the current state and its previous state. Linear systems are solved using the generalized minimal residual method (GMRES) technique. After numerical processing, temperature data collected by the numerical probes are compared with those in specific literature.

3 Contact resistance parameters

As mentioned above, the equation of the contact resistance used by COMSOL requires knowledge of the h_g, σ_{asp}, m_{asp}, H_c, and P parameters. The convection heat transfer coefficient adopted for air was 10 W/m^{2}K [35].

Roughness values were measured using a MarSurf M 400C roughness tester. With this device, the roughness of the cutting insert exit surfaces were measured with an ISO SNMG 120408 geometry, without chip breakage. To measure the

Table 1 Densities of WC, AISI 1045 steel, Al$_2$O$_3$, and TiN

Material	Specific mass ρ (kg/m^3)
Tungsten carbide	14100
AISI 1045 steel	7850
Al$_2$O$_3$	3900
TiN	5220

Table 2 Emissivity for AISI 1045 steel, Al$_2$O$_3$, and TiN

Material	Emissivity
AISI 1045	0.828
Al$_2$O$_3$	0.850
TiN	0.73

Table 3 Peak slope roughness and mean roughness values

Element	σ_{asp} (μm)	m_{asp}
Uncoated insert	0.205	0.106
Al$_2$O$_3$-coated insert	0.256	0.132
TiN-coated insert	0.199	0.127
Shim	0.205	0.113
Tool holder	0.518	0.109

Table 5 Calculation of H_c microhardness

Element	d (mm)	$A \times 10^{-10}$ (m^2)	F (kgf)	F (N)	H_c (GPa)
Uncoated insert	0.013875	1.93	0.2000	1.9619	10.19
Al$_2$O$_3$-coated insert	0.013380	1.79	0.2002	1.9635	10.97
TiN-coated insert	0.014285	2.04	0.010	1.9716	9.66
Shim	0.014785	2.19	0.2044	2.0051	9.17
Tool holder	0.027630	7.63	0.2001	1.9628	2.57

roughness of the tool holder surface, a Sandvik PCLNR 2525M 12 tool holder was used. The values obtained are shown in Table 3.

The durometer, from the Metallography Laboratory of the Universidade Federal Itajubá, was used to measure hardness. In this test, a load of 200 g is applied for 15 s through a diamond point at an angle of 136°. The indentation leaves a mark whose diagonals D_1 and D_2 are used to calculate the projected area. The hardness values are shown in Table 4.

The relationship between Vickers hardness and the force applied to the projected area is given by Eq. (10).

$$HV = \frac{2.F.sen(136°/2)}{d^2} \qquad (10)$$

in what HV is the Vickers hardness; F is the force applied in the projected area, in kgf; and d is the arithmetic mean of the D_1 and D_2 diagonals. From Eq. (10), the F applied forces in the hardness tests are obtained. The forces are then converted to N to calculate the parameter H_c for each set component. Table 5 shows the data of the elements of the set. In Table 5, H_c is obtained by the relation of the force, in N, with the respective indentation area, in m^2.

The last required parameter is the contact pressure P which is the result of the force exerted by the tightening of the screw, F_{app}, and the cutting force, F_c. According to Cunha [36], the F_{app} component is calculated from the geometric data of the screw and the tightening torque, being calculated by Eq. (11), with F_{app} being the tightening force of the screw, in N; T_{ap}, the tightening torque of the screw, in Nm; C_{ap} is the torque coefficient; and D_{np}, the nominal diameter of the screw, in m:

$$F_{app} = \frac{T_{ap}}{C_{ap}.D_{np}} \qquad (11)$$

The tightening torque was determined with a Calypso torque wrench with a resolution of 0.5 Nm and an operating range from 0 to 15 Nm. For non-lubricated assemblies, Cunha [36] indicates the torque coefficient of 0.15. The tool holder uses an M8 × 1.25 screw to fix the clamp, whose D_{np} value is 8 mm. Under such conditions, the tightening torque obtained is 4 Nm. The proportion of pressure due to cutting force can be calculated by Eq. (12):

$$F_c = K_s A_c \qquad (12)$$

in which F_c is the cutting force, in N; K_s is the specific cutting pressure, in N/mm^2; and A_c is the contact area between the workpiece and the insert, in mm^2. According to the manufacturer Sandvik, the specific recommended cutting pressure for the case is 1500 N/mm^2. Therefore, the portions that contribute to the contact pressure are shown in Table 6.

However, the contact pressure P is a ratio between the F_{app} and F_c forces described and the areas on which they are applied. The areas were calculated with the CAD program, except for contact area between insert and workpiece. In Fig. 10, the areas of each region of the insert are identified, and their respective values are shown in Table 7.

It is then considered that the entire clamping force of the screw is integrally transmitted through the clamping clamp to the insert. This means that deformations in the clamp are ignored. Furthermore, forces acting in the x and y directions are neglected. As a result, the contact pressure is the result of

Table 4 Vickers microhardness values

Element	Vickers microhardness (Hv)	D_1 (μm)	D_2 (μm)
Uncoated insert	1926.4	13.75	14
Al$_2$O$_3$-coated insert	2073.2	13.63	13.13
TiN-coated insert	1826.4	14.50	14.07
Shim	1733.9	14.82	14.75
Tool holder	486.0	27.63	27.63

Table 6 Parameters for calculating contact forces

Parameters	Force
T_{ap} = 4 Nm C_{ap} = 0.2	F_{app} = 3333.3N
D_{np} = 8 mm	
K_s = 1500 N/mm^2 A_c = 0.411 mm^2	F_c = 616.2 N
Total force	F_{tot} = 3949.6 N

Fig. 10 Areas A_1, A_2, and A_3 of the insert regions subject to contact pressure P

(a)   (b)
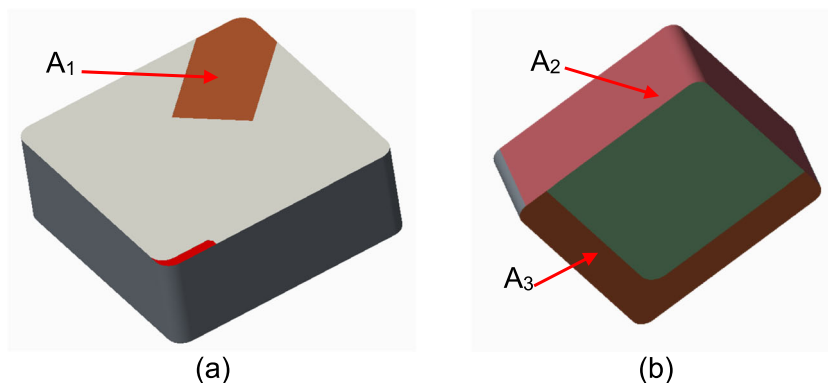
forces acting only in the z direction. It should be noted that area A_1 is subject only to the tightening force of the screw, while area A_3 is subject to the tightening force of the screw plus the cutting force. In this way, the contact pressures for each area are shown in Table 8.

4 Probe positions, direct problem solving, and evaluated cases

To follow the temperature evolution, numerical probes were inserted in the cutting insert, according to the coordinates shown in Table 9. These numerical probes are distributed in the first 10 μm, which is the thickness equivalent to that of the coating. In Fig. 11, the distribution of these probes is qualitatively represented. The R00 probe is positioned to calculate temperatures at the insert exit surface, at the interface between the chip and the insert on a real tool. The R10 probe is positioned 10 μm below the exit surface, equivalent to the interface between the coating and the substrate in cases where the coating presence is considered. This distribution of the probes is adopted in the coating and uncoating models. It is possible to compare the effects of different thermal properties of different materials on the temperature distribution in those first 10 μm.

For the solution of the direct problem and the calculation of temperatures, the estimated heat flux is using the nonlinear function specification method [9]. The machining conditions for which the heat flux was estimated are 0.138 mm/rev feed rate, 135.47 m/min cutting speed and 3 mm depth of cut, and

an initial temperature of 31 °C. The experimental procedure used in Brito et al. [9] was carried out in a city typically warm, hence the higher initial temperature. However, this higher temperature is small compared to the temperatures achieved on the exit surface at contact with piece. The heat flux profile is shown in Fig. 12. The heat flux was estimated for a period of 90 s, with a time increase of 0.5 s. Between $t = 9$ s and $t = 57$ s, the heat flux oscillates around a mean value, decreasing from $t = 57$ s to time $t = 90$ s.

Six cases were simulated, described below:

Case 1: Condition without coating and contact resistance;
Case 2: Condition with Al_2O_3 coating, without contact resistance;
Case 3: Condition with TiN coating, without contact resistance;
Case 4: Uncoated condition with thermal contact resistance;
Case 5: Condition with Al_2O_3 coating and contact resistance; and
Case 6: Condition with TiN coating and contact resistance.

5 Result analysis

To validate the numerical solution, the model in case 1 received a numerical probe R11, positioned at $xyz = (0, 3.95, -2.12)$ mm, which corresponds to one of the thermocouples used in the experiment of Brito et al. [9]. In Fig. 13a, the temperature calculated by probe R11 is compared with the experimental temperature measured in Brito et al. [9]. Fig. 13b shows the deviation between the numerical and experimental temperatures so that the deviation is calculated by Eq. (13):

$$Deviation = \left(\frac{T_{exp} - T_{num}}{T_{exp}}\right) * 100 \tag{13}$$

Table 7 Areas of contact interfaces between the elements of the set

Domain	Description	Area (mm^2)
A_1	Contact between insert and clamp	24.45
A_2	Side contact between insert and tool holder	110.17
A_3	Contact between insert and shim	50.84

Table 8 The portion of forces and contact pressure acting in the areas A_1, A_2, and A_3

Area	Clamping force	Cutting force (N)	Total force in the area (N)	Area (mm^2)	Contact pressure, P (MPa)
A_1	3333.3	0	3333.3	24.45	136.3
A_2	0	0	0	110.17	0
A_3	3333.3	616.3	3949.6	50.84	77.7

For probe R11, the maximum temperature calculated was 184 °C, at instant $t = 57$ s. The mean deviation was 3.8% and the maximum 22.6%, using a mesh of 283,337 elements.

5.1 Cases without contact resistance

Figure 14a shows the temporal evolution of the probe temperatures, which were calculated on the model exit surfaces. Uncoated and TiN coated temperatures are close. The temperature for the Al_2O_3 coated model is higher than in cases 1 and 3. The maximum temperatures calculated by the probes, in the three cases occur at time $t = 57$ s. Fig. 14b shows the temporal evolution of temperatures, calculated by probe R10 for the first three cases, as previously described.

The temperature along the z axis, at $t = 57$ s, is represented in Fig. 15. For this time, temperatures calculated by R00 probe are 769.9 °C, 810.9 °C, and 770.3 °C for cases 1, 2, and 3, respectively. Temperatures calculated by R10 probe, placed 10 μm below the exit surface, where the interface between coating and substrate would be, are 762.6 °C, 760.7 °C, and 758.1 °C, for cases 1, 2, and 3, respectively. Note that, for coated cases, the temperature in the substrate is lower than that obtained for case 1, which has no coating. Still in relation to Fig. 15, it is noted that for case 1, the temperature variation from 769.9 °C to 732.6 °C in 10 μm is equivalent to a temperature gradient of 3,740,000 °C/m. The second case, whose reduction was from 810.9 to 760.7 °C, is equivalent to a thermal gradient of 5,031,000 °C/m. In the third case, with TiN

coating, in the space of 10 μm, the temperature was reduced from 770.3 to 758.1 °C, which is equivalent to a temperature gradient of 1,219,000 °C/m.

The temperature profiles on the cutting tool external surfaces, at $t = 57$s, are shown in Fig. 16. Figure 16a presents the temperature field for case 1. At the contact interface, there are points with temperatures up to 820 °C. In Fig. 16b, the temperature field of case 2 is shown, whose coating is Al_2O_3. Due to this coating presence, temperatures of around 858 °C are observed at the contact interface. In Fig. 16c, the temperature field of case 3 is shown. Although there is a coating, the exit surface temperature differs little from the situation shown in Fig. 16a.

5.2 Contact resistance cases

The temporal evolution of the temperatures calculated by the probes on the model exit surfaces, for cases 4, 5, and 6, is shown in Fig. 17a. The temperatures of cases 4 and 6 show very similar behavior, while case 5 shows slightly higher temperatures. If compared with the three previous cases, the exit surface temperature in cases 4, 5, and 6 is higher due to the contact resistance. The calculated maximum temperatures also occurred at instant $t = 57$ s. Figure 17b shows the temporal evolution of the temperatures calculated by the R10 probe, placed 10 μm below the exit surface. The temperatures calculated by this probe in cases 4, 5, and 6 are close to each other but higher when compared with the temperatures calculated by the R10 probe in cases 1, 2, and 3.

Table 9 Positions of the numerical probes

Probe	x (mm)	y (mm)	z (mm)
R00	0.25	1.35	0
R01	0.25	1.35	−0.001
R02	0.25	1.35	−0.002
R03	0.25	1.35	−0.003
R04	0.25	1.35	−0.004
R05	0.25	1.35	−0.005
R06	0.25	1.35	−0.006
R07	0.25	1.35	−0.007
R08	0.25	1.35	−0.008
R09	0.25	1.35	−0.009
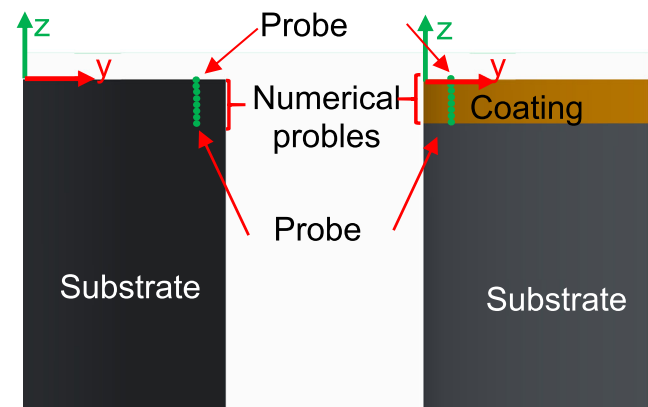
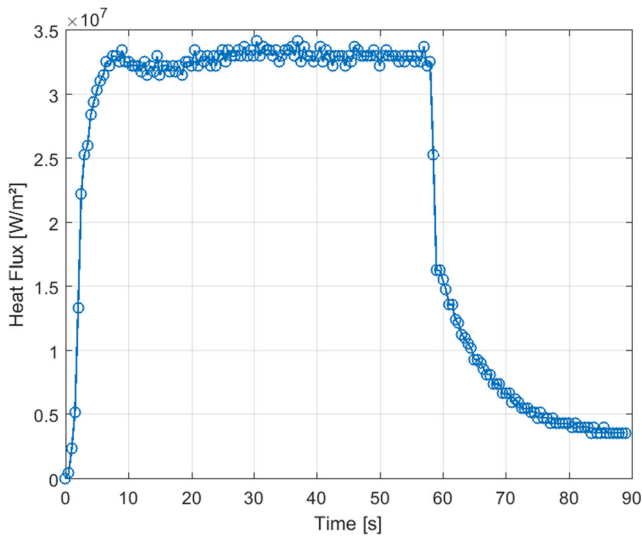**Fig. 11** Numerical probes position on the models

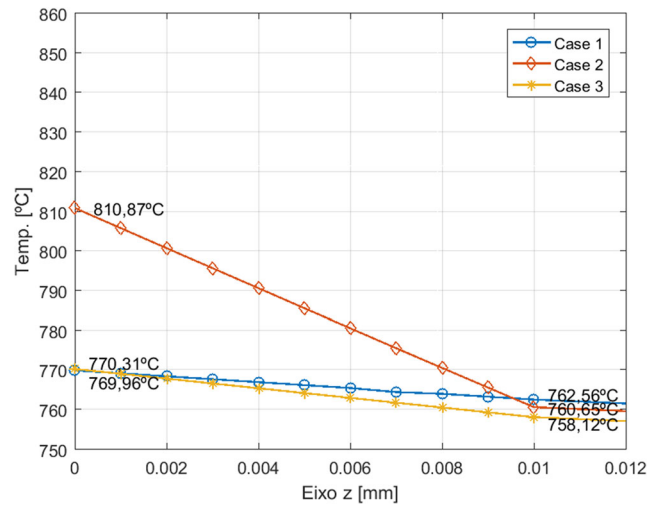**Fig. 12** Heat flow estimated by Brito et al. [9] used to solve the direct problem

Fig. 15 Comparison of coating temperatures, calculated for all numerical probes, at $t = 57$ s for cases 1, 2, and 3
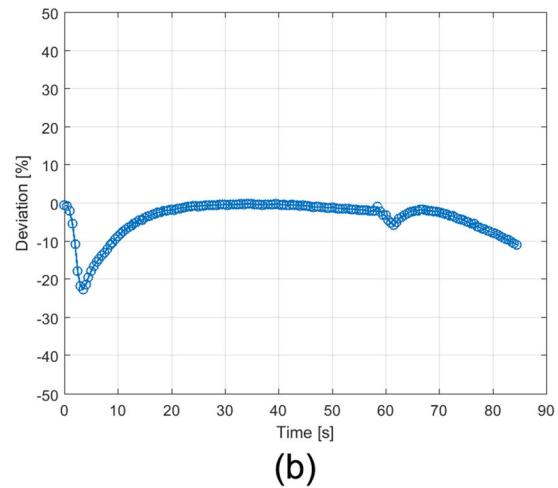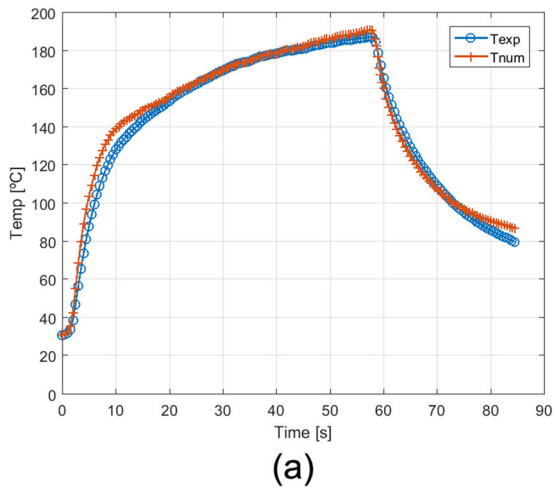

Fig. 13 Comparison between numerical and experimental temperature for validation (**a**) and deviation between numerical and experimental temperature (**b**)
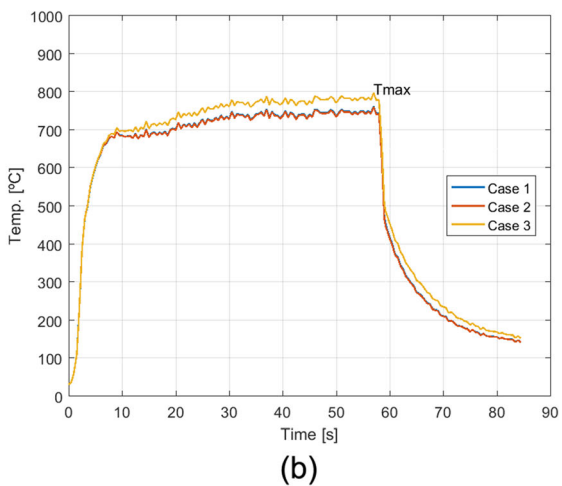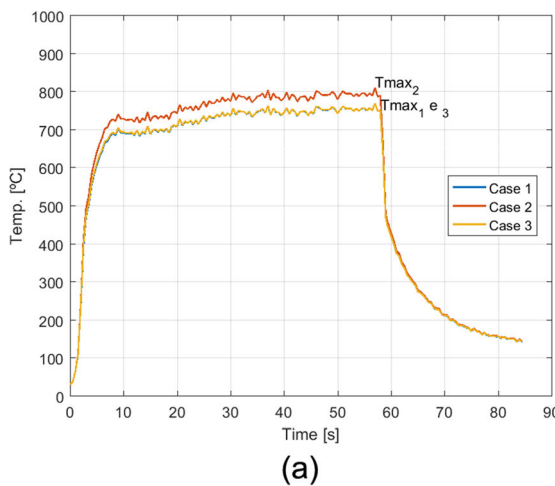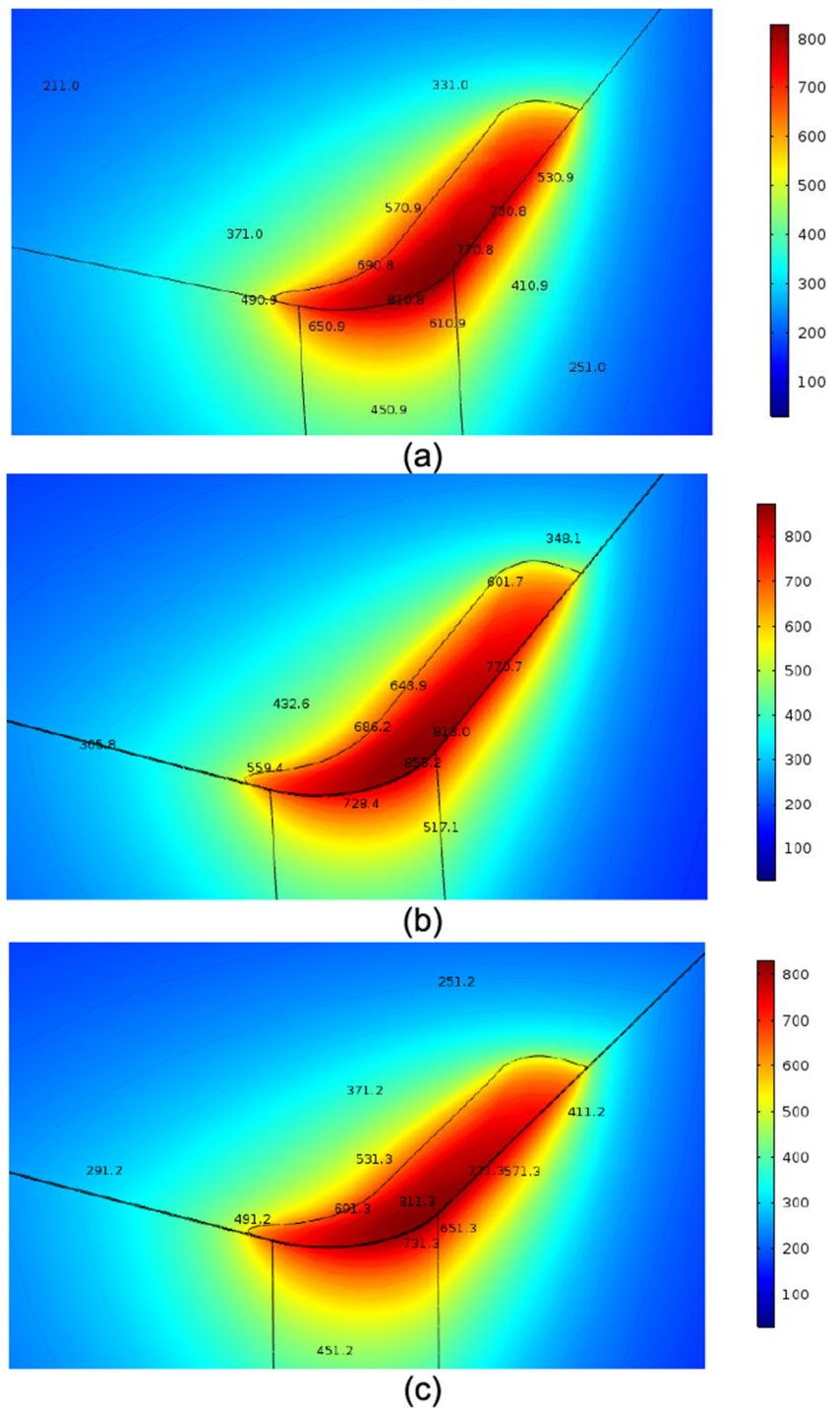

Fig. 14 Evolution of temperatures calculated, in the absence of contact resistance, by probe R00 (**a**) and probe R10 (**b**)

**Fig. 16** Tool temperature field at instant $t = 57$ s for case 1 (**a**), case 2 (**b**), and case 3 (**c**)

(a)

(b)

(c)

The maximum temperatures calculated by probe R00, at instant $t = 57$ s, were 815.0 °C, 851.8 °C, and 809.7 °C for cases 4, 5, and 6, respectively. The maximum temperatures calculated by the R10 probe, also at instant $t = 57$ s, were 807.7 °C, 800.0 °C, and 797.6 °C, for cases 4, 5 and 6, respectively.

The temperature reductions in the first 10 μm are shown in Fig. 18. According to the simulations, for case 4, the temperature varied from 815.03 to 807.73 °C in 10 μm, equivalent to a temperature gradient of 730,000 °C/m. In case 5, whose model is coated with Al_2O_3 and has contact resistance, the temperature, in 10 μm of material, was reduced from 851.8 to 800.3 °C, resulting in a temperature gradient of 5,155,000 °C/m. In the sixth case, in which the TiN coating is considered, there was also a temperature drop along the z axis. For this case, the temperature calculated at instant $t = 57$ s
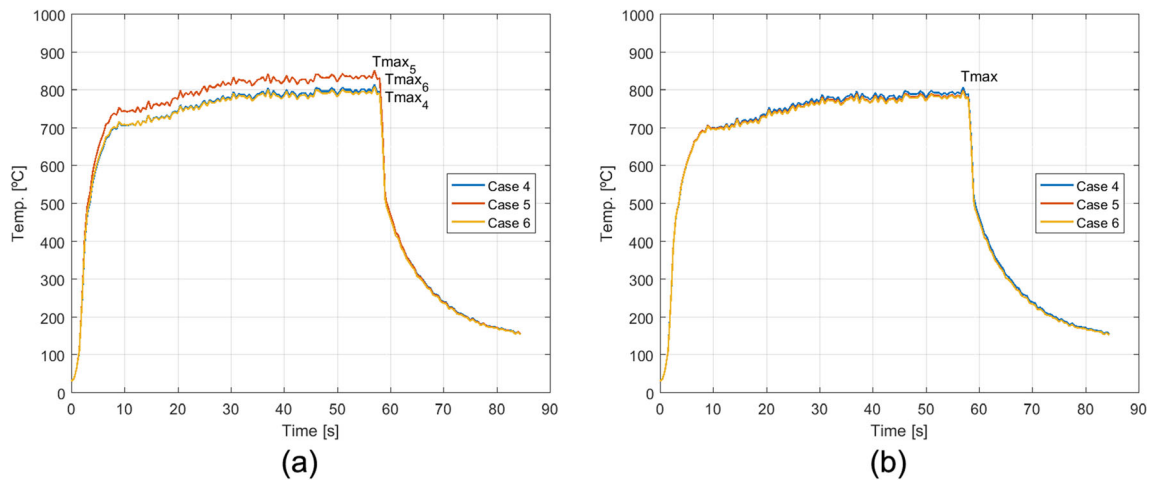
Fig. 17 Evolution of temperatures calculated by probe R00 (**a**) and probe R10 (**b**) considering contact resistance

for the exit surface by the R00 probe was 809.7 °C, equivalent to a temperature gradient of 1,207,000 °C/m.

Temperature fields, for the cutting tool exit surfaces, at instant $t = 57$s, are shown in Fig. 19. In Fig. 19a, the temperature distribution for case 4 is shown. In the contact interface, there are points with temperatures up to 858 °C. Fig. 19b shows the temperature field of case 5; due to the Al_2O_3 coating, points with temperatures of 898 °C are observed at the contact interface. In Fig. 19c, the temperature field of case 6 is shown, condition with TiN coating. In this case, there are points with temperatures above 810 °C.

One of the coating functions is to retain the heat of the chip shear and its friction with the cutting tool. In this case, less heat is directed to the substrate; thus, the cutting insert surface temperature increases. The coating effect on the temperature increase in the exit surface was evaluated by comparing the temperatures calculated by the R00 probe in cases 2 and 3 with the respective temperature in case 1 or by comparing the temperatures of cases 5 and 6 with case 4. In all these
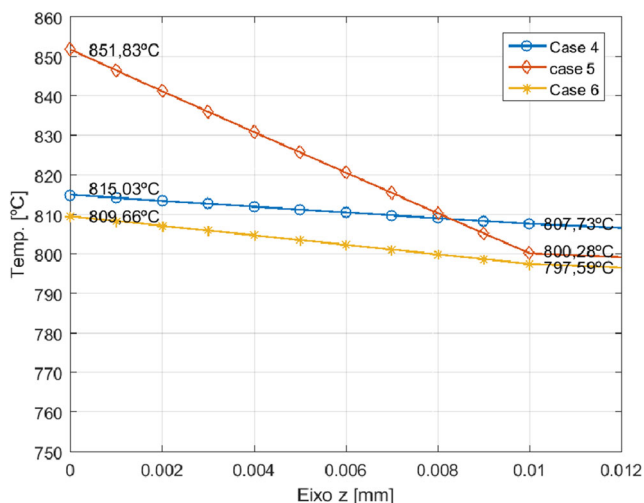
situations, the coating caused changes in the exit surface temperature compared to the cases without coating. In cases 2 and 3, the coating presence increased the temperature by 41 °C and 0.354 °C for Al_2O_3 and TiN, respectively, when compared with case 1. When considering the contact resistance, the presence of the Al_2O_3 coating caused an increase in the exit surface temperature of 36.8 °C. The TiN coating, on the other hand, showed a behavior opposite to that of Al_2O_3 concerning the temperature of the exit surface, causing a reduction of 5.3 °C. The effect of the coating could be evaluated in Fig. 15 and 18.

The coatings fulfill the function of softening the heat directed to the insert substrate but in different intensities and different ways. While Al_2O_3 acts as a thermal barrier, retaining heat at the exit surface, TiN presents a less intense temperature gradient in the space of 10 μm, including a lower temperature in the exit surface, as occurred in case 6.

The second parameter evaluated is the contact resistance, the effect of which is to reduce heat dissipation by the assembly, thereby retaining more heat in the cutting insert. According to the simulation results, the contact resistance changed the cutting insert temperature range (Figs. 15 and 18). The simple fact of including contact resistance raised the temperature at the exit surface by 45.1 °C, 40.9 °C, and 39.4 °C for uncoated tools and coated with Al_2O_3 and TiN, respectively. At the R10 probe point, the contact resistance presence caused a temperature increase of 45.2 °C, 39.6 °C, and 39.5 °C for inserts without coating and coated with Al_2O_3 and TiN, respectively.

Fig. 18 Comparison of coating temperatures, calculated on numerical probes, at instant $t = 57$ s for cases 4, 5, and 6

6 Conclusion

In this work, it was proposed to evaluate the temperature field in cutting tools for turning with and without coating. Along with this analysis of the coating, it was also analyzed the

Fig. 19 Temperature field at instant $t = 57s$ for case 4 (**a**), case 5 (**b**), and case 6 (**c**)
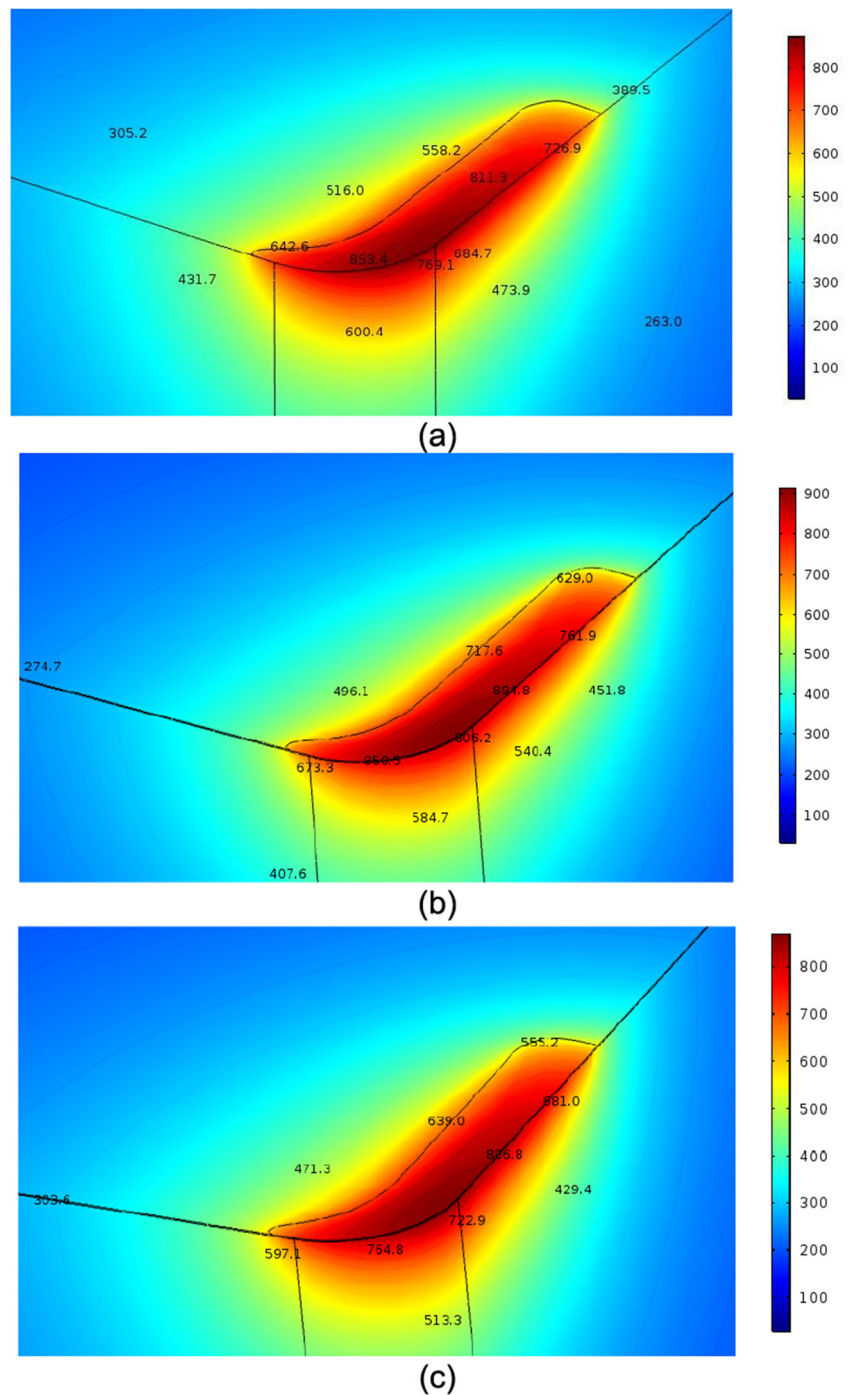
effects of contact resistance on the cutting tool heating. For this, the cutting and heating mechanisms of the tool were evaluated. Three insert conditions were simulated, which were as follows: uncoated and with Al_2O_3 and TiN coatings, respectively. Such cases were simulated first by neglecting the contact resistance and, in a second step, considering the contact resistance. For the studies of these cases, a real turning operation was considered, with a duration of 85.5 s.

Al_2O_3 acted as a thermal barrier in relation to the coating effect, causing an increase in temperature at the exit surface. Its specific heat, for temperatures close to 1000 K, is lower than ambient temperature. The specific heat of Al_2O_3 is reduced in the region where the heat flux is applied, contributing to raise the temperature at the exit surface. The TiN coating protects the substrate of the cutting insert by acting differently to the behavior of its thermophysical properties in relation to temperature. This material acquires the ability to conduct heat

with increasing in temperature, which makes the temperature at the beginning of the substrate lower than the uncoated tool. The temperature at the exit surface, in this case, on the other hand, does not rise due to its specific heat, which also increases almost linearly with temperature. Hence, the TiN acquires a higher thermal capacitance.

According to the simulations, the contact resistance negatively altered the temperature values in the cutting insert substrate by preventing heat dissipation. According to the simulations, the temperature at 10 μm below the exit surface increased in 45.2 °C, 39.6 °C, and 39.5 °C in the uncoated models Al_2O_3, and TiN concerning the cases without coating.

Therefore, the importance of considering the contact resistance to obtain more realistic values of the numerically calculated temperatures is emphasized. The use of COMSOL software was also essential for implementing all the methodology used to calculate the contact resistance. COMSOL allowed the main parameters responsible for contact resistance measured in this work to be considered in the thermal model for temperature calculation.

Availability of data and materials The datasets generated and/or analyzed during the current study are available from the corresponding author on reasonable request.

Author contribution Carlos Adriano Corrêa Ribeiro: conceptualization, methodology, software, formal analysis, and writing; João Roberto Ferreira: resources and co-supervision; and Sandro Metrevelle Marcondes de Lima e Silva: resources, review, editing, and supervision.

Declarations

Ethics approval The manuscript in part or in full has not been submitted or published anywhere, and the manuscript will not be submitted elsewhere until the editorial process is completed.

Consent to participate All the participated persons are listed in the article.

Consent for publication Approved.

Competing interests The authors declare no competing interests.

References

1. Shore H (1925) Thermoelectric measurement of cutting tool temperature. J Wash Acad Sci 15:85–88 https://www.jstor.org/stable/24527287

2. Chen G, Ren C, Zhang P, Cui K, Li Y (2013) Measurement and finite element simulation of micro-cutting temperatures of tool tip and workpiece. Int J Mach Tool Manu 75:16–26. https://doi.org/10.1016/j.ijmachtools.2013.08.005

3. Grzesik W, Nieslony P (2003) A computational approach to evaluate temperature and heat partition in machining with multilayer coated tools. Int J Mach Tool Manu 43:1311–1317. https://doi.org/10.1016/S0890-6955(03)00160-3

4. Iraola J, Rech F, Valiorgue F, Arrazola PJ (2012) Characterization of friction coefficient and heat partition coefficient between an austenitic steel AISI304L and tin-coated carbide cutting tool. Mach Sci Technol 16:189–204. https://doi.org/10.1080/10910344.2012.673965

5. Kaminise AK, Guimarâes G, Silva MB (2014) Development of a tool–work thermocouple calibration system with physical compensation to study the influence of tool-holder material on cutting temperature in machining. Int J Adv Manuf Technol 73:735–747. https://doi.org/10.1007/s00170-014-5898-0

6. Machado AR, Abrão AM, Coelho RT, Silva MB (2011) Teoria da usinagem dos materiais (in Portuguese), 2nd edn. Edgard Blucher, São Paulo

7. Rech J, Kusiak A, Battaglia JL (2004) Tribological and thermal functions of cutting tool coatings. Surf Coat Technol 186:364–371. https://doi.org/10.1016/j.surfcoat.2003.11.027

8. Aspinwall D, Mantle AL, Chan WK, Hood R, Soo SL (2013) Cutting temperatures when ball nose end milling γ-TiAl intermetallic alloys. CIRP Ann Manuf Technol 62:75–78. https://doi.org/10.1016/j.cirp.2013.03.007

9. Brito RF, Carvalho SR, Silva SMM LE (2015) Experimental investigation of thermal aspects in a cutting tool using comsol and inverse problem. Appl Therm Eng 86:60–68. https://doi.org/10.1016/j.applthermaleng.2015.03.083

10. Groover MP, Kane GE (1971) A continuing study in the determination of temperatures in metal cutting using remote thermocouples. J Ind Eng Int 2:603–608. https://doi.org/10.1115/1.3427967

11. Maliska CR (2004) Transferência de calor e mecânica dos fluidos computacional (in Portuguese), 2nd edn. LTC, Rio de Janeiro

12. Coroni DA, Croitoru SM (2014) Prediction of cutting force at 2D titanium machining. Procedia Eng 69:81–89. https://doi.org/10.1016/j.proeng.2014.02.206

13. Goodarzi K, Ramezani SR, Hajati S (2014) Reducing thermal contact resistance using nanocoating. Appl Therm Eng 70:641–646. https://doi.org/10.1016/j.applthermaleng.2014.04.028

14. Zheng J, Li Y, Wang L, Tan H (2014) An improved thermal contact resistance model for pressed contacts and its application analysis of bonded joints. Cryogenics 61:133–142. https://doi.org/10.1016/j.cryogenics.2013.11.002

15. Beake BD, Ning L, Gey C, Veldhuis SC, Komarov A, Weaver A, Khanna M, Fox-Rabinovich GS (2015) Wear performance of different PVD coatings during hard wet end milling of H13 tool steel. Surf Coat Technol 279:118–125. https://doi.org/10.1016/j.surfcoat.2015.08.038

16. Diniz AE, Marcondes FC, Coppini NL (2014) Tecnologia da usinagem dos materiais (in Portuguese), 4th edn. Artliber, São Paulo

17. Li W, Guo YB, Barkey ME, Jordon JB (2014) Effect tool wear during end milling on the surface integrity and fatigue life of inconel 718. Procedia CIRP 14:546–551. https://doi.org/10.1016/j.procir.2014.03.056

18. Wanglin C, Zheng J, Meng X, Kwon S, Zhang S (2015) Investigation on microstructures and mechanical properties of AlCrN coatings deposited on the surface of plasma nitrocarburized cool-work tool steels. Vacuum 121:194–201. https://doi.org/10.1016/j.vacuum.2015.08.021

19. Aiso T, Wiklund U, Kubota M, Jacobson S (2016) Effect of Si and Al additions to carbon steel on material transfer and coating damage

mechanism in turning with CVD coated tools. Wear 368-369:379–389. https://doi.org/10.1016/j.wear.2016.10.011

20. Bobzin K (2016) High-performance coatings for cutting tools. CIRP J Manuf Sci Tech 18:1–9. https://doi.org/10.1016/j.cirpj.2016.11.004

21. Krajinovic I, Daves W, Tkadletz M, Tappernegg T, Klünsner T, Schalk N, Mitterer C, Tritremmel C, Ecker W, Czetti C (2016) Finite element study of the influence of hard coatings on hard metal tool loading during milling. Surf Coat Technol 304:134–141. https://doi.org/10.1016/j.surfcoat.2016.06.041

22. Köpf A, Keckes J, Todt J, Pitonak R, Weissenbacher R (2017) Nanostructured coatings for tooling applications. Int J Refract Met H 62:219–224. https://doi.org/10.1016/j.ijrmhm.2016.06.017

23. Park ST, Han JG, Keunecke M, Lee K (2017) Mechanical and structural properties of multilayer c-BN coatings on cemented carbide cutting tools. Int J Refract Met H 65:52–56. https://doi.org/10.1016/j.ijrmhm.2016.11.009

24. Bar-Hen M, Etsion I (2017) Experimental study of the effect of coating thickness and substrate roughness on tool wear during turning. Tribol Int 110:341–347. https://doi.org/10.1016/j.triboint.2016.11.011

25. Vereschaka AA, Grigoriev SN (2017) Study of cracking mechanisms in multi-layered composite nano-structured coatings. Wear 378-379:43–57. https://doi.org/10.1016/j.wear.2017.01.101

26. Mo Y, Segawa S (2012) Thermal contact resistance measurements. J Enhanc Heat Transf 19:561–569. https://doi.org/10.1615/JEnhHeatTransf.2012006005

27. Cui T, Li Q, Xuan Y, Zhang P (2014) Multiscale simulation of thermal contact resistance in electronic packaging. Int J Therm Sci 83:16–24. https://doi.org/10.1016/j.ijthermalsci.2014.04.006

28. Cooper MG, Mikic BB, Yovanovich MM (1969) Thermal contact conductance. Int J Heat Mass Transf 12:579–300. https://doi.org/10.1016/0017-9310(69)90011-8

29. Carvalho SR, Silva SMM L e, Machado AR, Guimarães G (2006) Temperature determination at the chip-tool interface using an inverse thermal model considering the tool and tool holder. J Mater Process Technol 179:97–104. https://doi.org/10.1016/j.jmatprotec.2006.03.086

30. Grzesik W, Nieslony P, Bartoszuk M (2009) Modeling of cutting process analytical and simulation methods. Adv Manuf Sci Tech 33:5–29

31. Jiang F, Zhang T, Yan L (2016) Estimation of temperature-dependent heat transfer coefficients in near-dry cutting. Int J Adv Manuf Technol 86:1207–1218. https://doi.org/10.1007/s00170-015-8293-6

32. Polozine A, Schaeffer L (2005) Exact and approximate methods for determining the thermal parameters of the forging process. J Mater Process Technol 170:611–615. https://doi.org/10.1016/j.jmatprotec.2005.06.041

33. Wang YM, Tian H, Shen XE, Wen L, Ouyang JH, Zhou Y, Jia DC, Guo LX (2013) An elevated temperature infrared emissivity ceramic coating formed on 2024 aluminium alloy by microarc oxidation. Ceram Int 39:2869–2875. https://doi.org/10.1016/j.ceramint.2012.09.060

34. Hou J, Zhou W, Duan H, Yang G, Xu H, Zhao N (2014) Influence of cutting speed on cutting force, flank temperature, and tool wear in end milling of Ti-6Al-4V alloy. Int J Adv Manuf Technol 70:1835–1845. https://doi.org/10.1007/s00170-013-5433-8

35. Hahn DW, Özisik MN (2012) Heat conduction, 3rd edn. John Wiley & Sons, New Jersey

36. Cunha LB (2005) Elementos de Máquinas (in Portuguese), 1st edn. LTC, Rio de Janeiro